Multi-Scale Curvelet-Based Directional Denoising for Chest X-Ray Images

Neenu Sebastian*, B. Ankayarkanni
Department of Computer Science and Engineering-School of Computing,
Sathyabama Institute of Science and Technology (Deemed to be University), Chennai 600119, India

***Abstract*—In modern healthcare, medical imaging has a significant role in understanding the structure and functioning of the human body, which helps doctors to diagnose, to plan the treatment, and to monitor the disease. Chest X-rays are widely used for the early detection and treatment of various lung infections. The effectiveness and the accuracy of the diagnosis depend largely on the quality of the medical images. Chest X-rays often suffer from Gaussian and Poisson noise, which affects the visibility of fine anatomical structures. Although methods like Gaussian filtering, NLM, and GAN have been used, they often compromise between denoising and retaining edge details. A robust denoising algorithm, Multi-Scale Curvelet Filtering with Directional Denoising (MCF-DD), is proposed to denoise medical chest X-ray images, which uses the curvelet transform coefficients. The performance of the proposed MCF-DD model was evaluated on the Chest X-Ray Images dataset from the Kaggle repository and DICOM images from the MIDRC-RICORD-1C dataset. MCF-DD achieved a PSNR of 36.57dB and SSIM of 0.9062 on Kaggle images, and 40dB PSNR with 0.9412 SSIM on DICOM images, indicating strong denoising performance across both datasets.**

***Keywords*—Image denoising; medical image; Chest X-Ray; Poisson noise; Gaussian noise; Curvelet Transform**

I. Introduction

Medical images are used in healthcare for the diagnosis and monitoring of human diseases and health. Chest X-rays are of significant relevance in current medical diagnosis applications, as they are the most widely used cost-effective modality for diagnosing lung infections such as pneumonia, lung cancer, and COVID-19 [1]. The quality of chest X-rays is often compromised by the presence of noises such as Poisson and Gaussian noise [2]. The main sources of noise in X-ray images are scattered radiations, fluctuations in electronics, and quantum noise. To reduce the exposure of patients to ionizing radiation, low-dose imaging protocols that prescribe the usage of low photon count are used during medical imaging. Due to statistical variations in photon counts, Poisson noise gets added to X-ray images. As a result of these noises, the pixel distribution of the images will be altered, and this may result in the loss of image features such as texture, edges, intensity, etc. The presence of this noise affects the exact diagnosis and monitoring of the disease [3]. Enhancing the quality of Chest X-Ray images through effective denoising techniques is essential to support clinical procedures, as demonstrated by image-guided interventions that rely on clear imaging for precise treatment planning. So, image denoising is a required pre-processing stage for applications using medical images and so it is crucial to develop effective denoising techniques. Also, reliable denoising of chest X-rays under mixed Poisson and Gaussian noise remains a key challenge. Existing methods often fail to effectively suppress noise while preserving fine anatomical structures that are critical for accurate pneumonia diagnosis.

The various noise reduction methods can be broadly classified into four categories: conventional filtering, transform domain filtering, deep learning-based methods [4], and hybrid models [5]. For denoising, the conventional filtering methods use linear filters such as a Gaussian filter, mean filter, etc., and nonlinear filters such as a median filter [6], bilateral filter, etc. These filtering methods have low computational complexity, but the denoised images will be blurred, resulting in low resolution. In transform domain filtering, different transform functions are used to remove image noise. The advantages of transform methods include edge preservation and multi-resolution analysis, but after denoising using transform methods, the resultant image may contain artifacts that occur as a result of poorly chosen parameters and threshold values. Deep learning-based denoising methods use neural network architectures, particularly convolutional neural networks, autoencoders, and generative models, to learn complex noise patterns directly from data [7]. These approaches can adapt to various noise distributions and often outperform traditional techniques in preserving fine structural details. However, their performance heavily depends on the availability of large, high-quality annotated datasets, and they typically require significant computational resources for training and inference. Hybrid denoising models integrate multiple techniques, typically combining conventional or transform domain methods with deep learning approaches to exploit the strengths of each technique. These models aim to enhance denoising accuracy and robustness across diverse noise types. Recent studies report that deep learning methods show poor generalization across scanners, dose levels, and patient subgroups, and may cause over-smoothing or hallucinated textures in chest X-rays.

The above-discussed methods exhibit limitations such as blurring in conventional filters to data dependency in deep learning models. So, there is a need for an adaptive and structure preserving denoising framework for Chest X-Ray images. To address these challenges, Multi Scale Curvelet Filtering with Directional Denoising (MCF DD) framework is proposed. MCF DD employs curvelet based dynamic thresholding, which adaptively suppresses noise while preserving edge and texture details across scales and directions.

*Corresponding author

To overcome the lack of orientation-sensitivity in traditional methods, Gabor and Morlet filters are integrated to enhance directional and frequency-specific features. The inclusion of an anisotropic Gaussian filter ensures edge-preserving smoothing, minimizing the risk of blurring diagnostic boundaries. Unlike deep learning models, MCF DD does not rely on large annotated datasets or intensive training, offering a computationally efficient solution. Furthermore, by performing coefficient-level fusion of multiple filtered outputs, MCF DD combines the strengths of each component filter, achieving superior denoising performance without the architectural complexity of conventional hybrid models.

Unlike existing methods that rely on fixed global filtering, the proposed MCF-DD uses patch-wise adaptive noise characterization to guide noise-specific directional curvelet denoising, enabling effective handling of spatially varying mixed noise. In the proposed approach, a patch transformation method is applied where the input image patches are obtained by segmenting the input image, which is then fed as an input to the proposed robust denoising algorithm, Multi-Scale Curvelet Filtering with Directional Denoising (MCF-DD). In this algorithm, to capture the different anatomical structures, a multi-scale representation is needed, which can be achieved by using Curvelet Transform. By using Curvelet Transform, the input patches are divided into different scales and orientations, which helps to get the information regarding the local and global structure. To preserve the edge information, Curvelet Transform is integrated with directional filtering techniques: Gabor, Morlet, and Anisotropic Gaussian filters. This approach aims to effectively remove noise such as Gaussian and Poisson while preserving critical anatomical structures and features across multiple scales and orientations.

In summary, the key contributions of the proposed framework can be outlined as:

- A novel multi-scale denoising approach (MCF-DD) is proposed, which integrates curvelet-based multi-resolution decomposition with directional filtering to preserve structural details and suppress diverse noise types in chest X-rays.
- An initial patch-based classification mechanism is introduced that adaptively processes regions with varying noise intensities, reducing unnecessary computation and enhancing local feature preservation.
- For experimental validation, the model was tested on JPEG format chest radiographs from the Kaggle Chest X-ray dataset [8] and DICOM images from the MIDRC-RICORD-1C dataset [9]. The inclusion of both compressed and uncompressed formats ensures robustness of the proposed method across different imaging standards.

II. Related Work

Image denoising refers to the methods used to find the clear image from the noise image, as depicted in Fig. 1. The aim of denoising methods is to remove the noise from medical images and also to preserve the clinical details. According to the evaluation criteria outlined in [10], effective image denoising should maintain uniformity in flat regions, preserve edge sharpness without blurring, retain structural and textural details, keep the original contrast intact, and avoid introducing any unnatural artifacts.

In medical imaging, the different sources of noise can be low light, sensor characteristics, dust particles in scanning machines, disturbance in transmission channels, etc. The predominant types of noise encountered in medical images include Gaussian noise and Poisson noise. Gaussian noise is a type of noise that follows a Gaussian distribution [11]. Gaussian noise can be caused by different sources, such as sensor temperature fluctuations, low radiation dose, etc. Poisson noise is caused by the photon emission in Chest X-Rays. The variance of Poisson noise depends on image signal intensity. Chest X-Ray images and CT images usually contain a combination of Gaussian and Poisson noise. Various methods have been suggested to accomplish these denoising goals, ranging from traditional image processing methods to modern machine learning approaches. These methods are broadly categorized into conventional filtering, transform-based techniques, deep learning approaches, and hybrid models.

A detailed study of the application of filtering algorithms for denoising images is done in [12]. It is the most widely used denoising method. Filtering methods use mathematical models to remove noise from images. The linear filter works by computing the weighted sum of pixel values in a defined neighborhood. Gaussian[13] and mean filters are examples of linear filters that will remove the noise, but result in blurred denoised images. Median filter [14], Bilateral filter [15], and non-local means filter [16] use nonlinear adaptive filtering techniques to remove noises from images. They are better in preserving the edge information than the linear filters. In [17], advanced filtering techniques such as an adaptive Wiener filter are proposed, which generate less blurred denoised images compared to the other methods. An iterative process to reduce noise is proposed in [18], which results in better edge preservation while maintaining image quality.

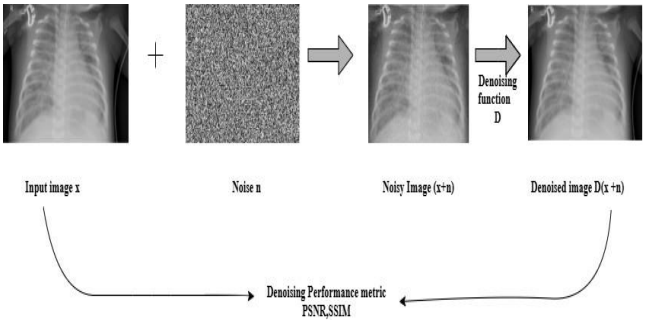

Fig. 1. Medical image denoising

Gaussian and Poisson noises are common types of noise affecting medical images. Filtering approaches work well for a particular type of noise, and their performance degrades for mixed noise [19]. So, there is a need for a denoising method capable of handling multiple types of noise.

In transform-based methods, to separate the noise and signal components, the image is converted from the spatial model to the mathematical model, where the noise and signals

have different frequency components. To suppress the frequency components of the noise, filtering or threshold methods are applied which preserve significant image structures. In Wavelet Methods [20], the wavelet threshold method was proposed, in which wavelet decomposition is used to separate noise from image signals, enabling adaptive noise removal with minimal loss of information. This method resulted in the over-smoothening of important anatomical features, as it captures only point singularity information rather than complex structural information. Adaptive Bayes Shrink thresholding [21] was proposed, in which the noise variance is calculated in each sub-band using the Bayesian estimation, which is used for the calculation of the optimal threshold value, which varies according to the noise level present in each band. DWT is an inconsistent noise removal method due to its shift variant property, in which a small shift in the image information leads to the generation of different wavelet coefficients. In [22], Stationary Wavelet Transform (SWT), which addresses the shift variant property of DWT, is proposed by eliminating down-sampling, which is done by using the unsampled filter coefficients and convolution. The increased computational cost and redundancy make it less suitable for real-time processing of medical images. The other transform-based methods are Curvelet Transform (CT) [23], [24], Contourlet Transform (CTT) [25], Shearlet Transform (ST) [26]. Transform-based methods handle Gaussian noise, but they have limitations when handling Poisson noise due to the signal's dependent nature.

Deep learning methods are widely used for medical image denoising due to their capability for automatic feature extraction. Specific noise models, which are used in traditional methods, limit their ability to adapt to mixed noise input images, while deep learning approaches learn the noise patterns from noisy images, which are later used for noise removal. A deep CNN model for handling the Gaussian noise using residual learning is proposed in [27]. A self-supervised learning method that removes Poisson noise in CT images was proposed in [28]. The requirement of multiple noisy images of the same patient challenged the efficiency of this method in medical imaging. Autoencoder-based approaches were proposed in the work [29]. In [30], an efficient deep learning model to estimate a residual image from the input image with the Gaussian noise was proposed. In GAN-based methods, an image-to-image translation approach for CT images was proposed in [31], [32]. The lack of paired training data, overfitting on small datasets, and high computational complexity challenge the application of deep learning methods for medical image denoising.

For achieving better results, several researchers have proposed hybrid approaches, in which different denoising methods with different strengths are combined together. In [33], BM3D (Block Matching and 3D filtering) and wavelet transforms have been combined together which yields better textural preservation and fine details. But this method demanded a larger memory space requirement due to 3D filtering in BM3D. In [34], the CNN's ability to learn complex patterns is combined with wavelets' multi-scale representation. Several other hybrid models have been discussed in the work [35]. Hybrid methods give better results than single method, but the need of extensive training data, need of parameter tuning, and increased computational complexity limits its application. Inspired by these approaches, the proposed work aims to improve Chest X-Ray denoising by preserving critical anatomical structures and enhancing image quality. Though there are significant developments in medical image denoising techniques, there are several challenges that are to be addressed. One major challenge is the lack of a denoising technique that can effectively handle the mixed noise types that are often present in real-world medical imaging. Another challenge is the high computational complexity of particularly deep learning and hybrid methods, which will make them less practical for medical applications. There exist numerous studies for denoising MRI and CT images, and there is a noticeable lack of research in denoising X-Ray images. Among the various medical image modalities available, this research work focuses on Chest X-Rays, which are used for the detection and diagnosis of chest infections. This study presents a novel denoising framework, Multi-Scale Curvelet Filtering with Directional Denoising (MCF-DD), specifically designed to address critical gaps in existing medical image denoising techniques. Unlike conventional, deep learning, or hybrid approaches, the proposed method effectively handles mixed noise types, which commonly affect real-world chest X-rays. By focusing on the underexplored modality of chest radiographs and prioritizing both effective noise suppression and structural detail preservation, MCF-DD introduces a practical and domain-specific solution for enhancing diagnostic quality in resource-constrained clinical settings. Recent diffusion-aware frameworks, such as DIFCNet, utilize diffusion features or reconstruction inconsistencies learned through deep generative models to characterize image degradations. In contrast, the proposed MCF-DD framework is a non-learning, noise-adaptive method that directly targets mixed Poisson Gaussian noise through patch-wise statistical characterization and directional curvelet domain filtering, making it computationally efficient.

III. Proposed Methodology

The overall workflow of the proposed Multi-Scale Curvelet Filtering with Directional Denoising (MCF-DD) framework is illustrated in Fig. 2. For denoising medical images, a new method is proposed by leveraging a multi-scale Curvelet Transform integrated with directional filtering techniques such as Gabor, Morlet, and Anisotropic Gaussian filters. This approach removes both Gaussian and Poisson noise, while preserving critical anatomical structures and features across multiple scales and orientations. Poisson noise is signal-dependent and arises from the statistical nature of X-ray photon detection, making it more prominent in low-dose imaging, where fewer photons reach the detector. In contrast, Gaussian noise is signal-independent and typically originates from electronic imperfections in imaging systems. While Poisson noise affects areas with low photon counts, Gaussian noise is uniformly distributed across the image. Both types of noise degrade image quality by reducing contrast and obscuring anatomical details. Denoising methods like wavelet transforms, CNN-based approaches, and filtering techniques are often employed to mitigate these noise effects.

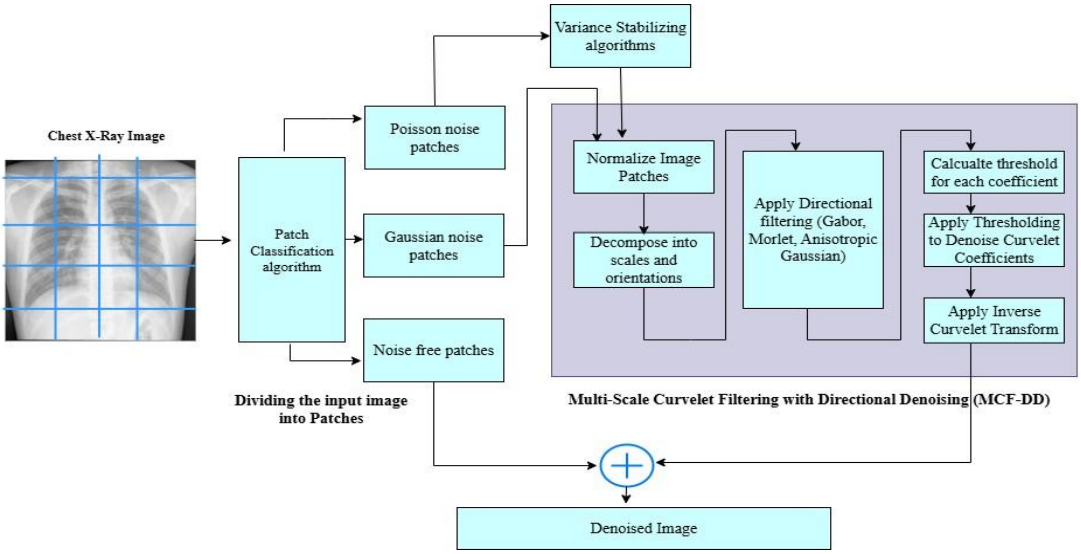

Fig. 2. System architecture

A. Patch Classification

In medical X-rays, preserving and enhancing edges and fine anatomical details is crucial for accurate diagnosis and interpretation. Conventional denoising and feature extraction methods, such as Gaussian filtering or basic wavelet transforms, often struggle to maintain these important features. The Curvelet Transform, on the other hand, represents images in terms of localized, oriented, and scale-specific components, which align better with the curvilinear structures typically present in biological tissues. To preserve and enhance subtle edges and fine anatomical details, the input medical image is divided into different patches of size 64 X 64. Each patch is analyzed to find the type of noise dominant in that patch, and correspondingly, the patch is classified into the following classes, such as the Gaussian class, Poisson class or noise-free image patch class. The noise-free image patches are preserved without any modifications and processing. The Poisson class patches will undergo Variance Stabilizing Transformations (VST) to transform the Poisson noise into a form where the variance becomes more uniform. The stabilized Poisson patch and the Gaussian noise patch will be given as input to Multi-Scale Curvelet Filtering with Directional Denoising (MCF-DD) for noise removal from the noisy image patches. The denoised image patches are aligned along with the noisy free patches to reconstruct the denoised image.

The medical image is divided into smaller, non-overlapping patches to analyze and process localized regions independently. This approach allows for identifying noise characteristics and applying appropriate denoising techniques at a granular level. This patching method enhances the ability to denoise the image efficiently while maintaining critical anatomical features. Each input image is divided into non-overlapping square patches of size 64 × 64 pixels. Prior to division, image dimensions are checked to ensure compatibility with the patch size. If the height or width is not perfectly divisible by 64, zero padding is applied to the bottom or right edges of the image. Each patch is analyzed for the dominant noise present in it. The difference in the characteristics of Gaussian and Poisson noises is used to calculate the dominant noise in the patches. Gaussian noises are uniform across all intensities. Gaussian noises will have high variance but are independent of the mean intensity. On the other hand, for Poisson noise, its variance increases proportionally to the mean intensity. Noise-free patches will have low variance-to-mean ratio. For an image patch with ‘n’ no pixels and if ‘li’ is the intensity of pixel i, the mean values of the patch ’m’ can be calculated using Eq. (1) [36]:

$$m = \frac{1}{n}\sum_{i=1}^{n} l_i \quad (1)$$

The measure of the spread of pixel intensities around the mean value gives the variance value ‘v’ of the patch which can be calculated using Eq. (2) [37]:

$$v = \frac{1}{n}\sum_{i=1}^{n}(l_i - m_i)^2 \quad (2)$$

Variance to Mean ratio (v_to_m_ratio) for image patch can be calculated using Eq. (3) [37]:

$$v_{to\_m\_ratio} = \frac{v}{m} \quad (3)$$

For classifying the image patches into Gaussian, Poisson and clean image clusters, Gaussian Mixture Model is used, which represents the data as mixture of multiple Gaussian distributions. In noisy Chest X-Ray image, the variance to mean ratio for image patches follows a multi modal distribution as the variance to mean ratio value’s characteristics changes depending on the type of noise dominant in that patch. GMM (Gaussian Mixture Model) is used to understand the data distribution and to determine the threshold values for classification. These threshold values dynamically vary depending on the data distribution characteristics. To fit a mixture of Gaussian distributions to variance to mean ratio, GMM initialize three Gaussian components for clean patches, Poisson patches and Gaussian patches, respectively. Then it uses Expectation Maximization algorithm [38] to adjust and improve the parameters such as mean (μ), variance (σ2), and weight (w). The mean values of the established three Gaussian distribution indicate the typical values for clean patches,

Poisson noise patches, and Gaussian noise patches, respectively. Algorithm 1 presents the patch classification.

Algorithm 1: Patch Classification Algorithm

Normalize the input image by scaling the pixel values to [0,1].

Extract *p_size* X *p_size* patches from the image.
Calculate the variance-to-mean ratio for each image patch.
Determine the dynamic thresholds T1, T2 using Gaussian Mixture Model (GMM), by fitting a 3 component GMM to the V/M ratios and use cluster means to set T1, T2.
For all image patches do
Compute mean and variance for the patch.
Compute *v_to_m_ratio.*
If *v_to_m_ratio*≥*T*2then
Assign to Gaussian_noise_patches
else if *T*1 ≤ *v_to_m_ratio* ≤ *T*2 then
Assign to Poisson_noise_patches
Else
Assign to Clean_patches
end if.
End

The thresholds T1 and T2 are then calculated as the midpoints between the adjacent Gaussian means to establish decision boundaries between the noise classes. T1 is set as the average of the mean values of the clean and Poisson noise distributions, and T2 is calculated as the average of the Poisson and Gaussian noise distributions. This adaptive thresholding approach ensures that the classification boundaries are not arbitrarily chosen but instead dynamically adapt to the distribution of noise in the dataset. The patches whose variance-to-mean ratio is greater than T2 are classified as Gaussian patches, and the patches with their variance-to-mean ratio between T1 and T2 are classified as Poisson patches. Patches with a variance-to-mean ratio less than T1 are classified as clean patches. Unlike a fixed threshold, GMM-based thresholds account for variations in image intensity ranges and different noise levels, making the method more robust and dataset independent.

The Poisson noise patches are transformed to Gaussian noise characteristics by applying a variance stabilizing technique called Anscombe transformation [39], which can be mathematically represented using the following Eq. (4) [39], where 'X' is the Poisson noise and 'Y' is the transformed noise signal, which resembles Gaussian noise, as the variance is stabilized.

$$Y = 2\sqrt{X + \frac{3}{8}} \tag{4}$$

To qualitatively support the GMM-based noise categorization, visual examples of image patches exhibiting different noise characteristics are displayed in Fig. 3. These patches, extracted from Chest X-Rays, represent samples categorized into distinct Gaussian components by the GMM. Each cluster corresponds to a different noise, such as clean patches, Gaussian patches and Poisson patches. The visual distinction in texture and granularity supports the adaptive noise categorization capability of the proposed algorithm.

B. Multi-Scale Curvelet Filtering with Directional Denoising (MCF-DD)

Medical images contain anatomical structures of varying sizes, like small cellular structures to large-scale structures like organ boundaries. In Chest X-Ray images, structures such as the lung trachea, Primary Bronchi, Bronchial Tree, and lungs constitute the larger structures, and small blood vessels, Alveolar Sacs, Bronchioles, and Capillaries are examples of smaller structures. So, it's necessary to have a multi-scale approach that retains and preserves both the small-scale and large-scale features. Also, the noise in medical images can be present at different scales, so a multi-scale approach is proposed, which addresses noise at each scale independently.

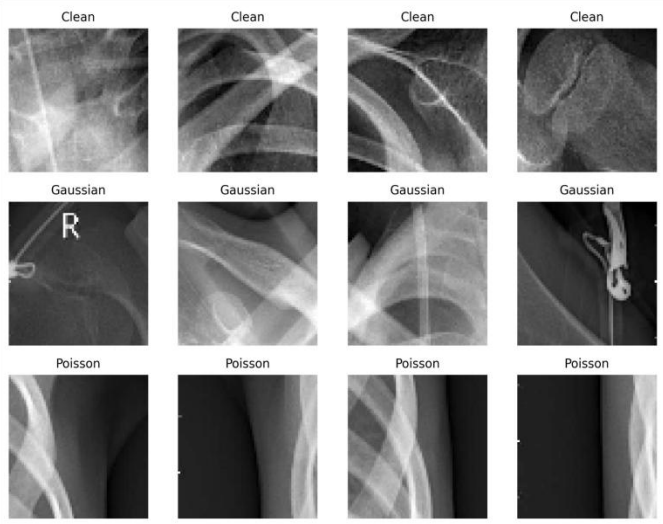

Fig. 3. Representative image patches from different Gaussian components identified by the GMM. Each row shows patches associated with a distinct noise category.

In Curvelet Transform, the images are decomposed into multiple scales and orientations, which captures both the small-scale and large-scale information in the X-Ray image. The Curvelet Transform outperforms the other mathematical transforms in capturing edges, curves, and fine details in images, which is particularly useful for medical imaging. It offers better edge preservation compared to other transforms. Algorithm 2 presents the MCF-DD Denoising algorithm. The different steps in Curvelet Transform are the following:

1) Decomposition: The Curvelet Transform decomposes the image into several sub-bands. Each sub-band captures the information in a specific orientation and scale. As a result of decomposition, the image is divided into multiple scales, where each scale corresponds to a different level of detail. Each scale contains multiple orientations that capture the edge and curve information in different directions like horizontal, vertical and diagonal. The mathematical representation of decomposition can be represented by Eq. (5), in which N (X, Y) the noisy image patch which is decomposes to 'S' number of scales with 'O' Orientations in each scale.

$$N(X,Y) \approx \sum_{s=1}^{S} \sum_{o=1}^{O} C_{s,o}(X,Y) \tag{5}$$

Algorithm 2: MCF-DD Denoising Algorithm

Apply Variance Stabilizing Transform (VST) to convert Poisson noise to a Gaussian-like distribution:

$$Y'=T(Y)$$

Perform Curvelet Decomposition on Y' using Fast Discrete Curvelet Transform (FDCT):

$$\Theta_Y = C(Y')$$

for all curvelet sub-bands $\theta_i \in \Theta_Y$ do

Apply directional filters (Gabor, Morlet wavelet, Anisotropic Gaussian) to θ_i

Estimate adaptive threshold τ_i using local statistics.

Apply thresholding to obtain denoised coefficients:

$$\hat{\theta}_i = F(\theta_i, \tau_i)$$

Reconstruct the image from denoised coefficients:

$$\hat{Y'} = C^{-1}(\hat{\Theta}_Y)$$

Apply inverse variance stabilizing transform to get the final denoised image:

$$\hat{X} = T^{-1}(\hat{Y'})$$

return $\hat{X}$

End

2) Apply directional filtering to each sub-band: Directional filtering is applied to each sub-band, in different scales and orientations, to capture localized curve and edge details. In chest X-Ray images, as both the fine and larger details have to be preserved, a combination of Gabor filter, Morlet filter, and Anisotropic Gaussian filters is used. This combination of filters provides the best trade-off between accuracy, detail preservation, and computational efficiency.

a) Gabor filter: Gabor filter [40], [41] captures the orientation and scale-specific information like edges, textures, and curved structures in images. Multi-orientation Gabor filters with orientations at 0°, 45°, 90°, and 135°, and a fixed frequency of 0.25 cycles/pixel are applied. They are used for texture analysis and feature extraction. Gabor filters are mathematically described by the following Eq. (6) [41]:

$$G(x,y) = \exp\left(-\frac{x^2+\gamma^2y^2}{2\sigma^2}\right)\cos\left(2\pi f \cdot (x\cos\theta + y\sin\theta)\right) \quad (6)$$

where,

θ - Orientation of the Gabor filter.

σ -Gaussian envelope's standard deviation.

f- Frequency of the sinusoidal component.

b) Morlet filter: Morlet filter [42] is used to capture localized frequency and orientation information. It combines a Gaussian window with a sinusoidal oscillation. They provide scale and orientation selectivity and so they are preferred for detecting features at multiple scales. Standard 2D complex Morlet wavelets were applied centred around a spatial frequency of 0.8 with a bandwidth parameter of 1. Morlet filters are mathematically described by the following Eq. (7) [42]:

$$\psi(x,y) = \exp\left(-\frac{x^2+y^2}{2\sigma^2}\right)\cdot\exp(j2\pi f_0 x) \quad (7)$$

where,

σ - Gaussian envelope's standard deviation.

f0 - Wavelet Central frequency.

j - Imaginary unit (j2= −1).

x, y - Spatial coordinates.

c) Anisotropic Gaussian filter: Anisotropic Gaussian filter [43] is used for directional smoothing by adjusting the standard deviations in different axes. These filters are better at maintaining anatomical boundaries and ensuring noise reduction without losing critical details. These were applied with a variable standard deviation across directions to enhance the preservation of directional edges as given by Eq. (8) [43]:

$$G(x,y) = exp\left(-\left(\frac{x^2}{2\sigma_x^2}+\frac{y^2}{2\sigma_y^2}\right)\right) \quad (8)$$

where,

Σx - X-direction Standard Deviation

Σy - Y-direction Standard Deviation

(x, Y) - Spatial Coordinates

3) Threshold calculation for denoising in curvelet transform: After obtaining the Curvelet coefficients, a threshold value for each coefficient to suppress noise is calculated. The noise thresholding technique for denoising was implemented using the median absolute deviation (MAD) method, as proposed in [44]. This method is effective for estimating noise variance in the transformed domain. Specifically, the noise level $\hat{\sigma}$ is estimated from the finest scale of Curvelet coefficients using Eq. (9) [44]:

$$\hat{\sigma} = \frac{\text{median}(|C_{i,j}|)}{0.6745} \quad (9)$$

where, $C_{i,j}$ are the Curvelet coefficients at the highest frequency scale. A universal threshold is then computed using Eq. (10) [44]:

$$T = \hat{\sigma}\sqrt{2\log N} \quad (10)$$

With N being the number of coefficients in the sub-band. Hard thresholding is applied by comparing the squared magnitude of each coefficient to the threshold. If $|C_{i,j}|^2 < T^2$, the coefficient is set to zero; otherwise, it is retained as given in Eq. (11) [44]:

$$\widehat{C_{i,j}} = \begin{cases} 0, if\left|C_{i,j}\right|^2 < T^2 \\ C_{i,j}, Otherwise \end{cases} \quad (11)$$

This operation removes insignificant coefficients likely representing noise while preserving meaningful structural details. The denoised image is then reconstructed using the inverse Curvelet Transform.

4) Reconstruction of the image: After denoising, reconstruction of the image is done by performing the Inverse Curvelet Transform, as given by Eq. (12) [45]. The denoised image patch is created back from the modified Curvelet

coefficients. The inverse transform aggregates all the scales and orientations back into the original pixel grid while retaining the geometrical structures. The reconstruction ensures that both edges and curves remain intact and the essential features are preserved.

$$\hat{f}(x,y) = C^{-1} \sum_s \sum_\theta \sum_k c_{s,\theta,k} \psi_{s,\theta,k}(x,y) \quad (12)$$

where,

C−1 is the inverse Curvelet Transform.

cs,θ,k is the Curvelet coefficients at scale s, orientation θ, and position k.

ψs,θ,k(x, y) is the Curvelet basis functions.

The summation is performed over all scales s, orientations θ, and positions k.

C. Patch Reconstruction

An empty image with the same size as original image is initialized. A weight matrix is maintained for keeping track of the number of patches contributing to each pixel. The denoised patches are placed in their original locations. The weight matrix is updated to normalize the overlapping regions. The reconstructed image is normalized using the weight matrix to maintain the consistency in intensities.

D. Parameter Settings and Selection Principles

The key parameters used in the various stages of the proposed Multi-Scale Curvelet Filtering with Directional Denoising (MCF-DD) framework are listed in Table I. The selection of each parameter was guided by a combination of empirical validation, literature references, and optimization trials to ensure robustness and optimal denoising performance. Gabor and Morlet parameters were chosen to ensure effective multi scale texture representation, while anisotropic Gaussian values were fixed to balance noise suppression and edge preservation. The dynamic thresholds were computed adaptively from the statistical distribution of curvelet coefficients, ensuring data-driven noise separation reproducibility. The curvelet transform was implemented using the wrapping-based discrete formulation, and sub-band coefficients were processed with a GMM-based adaptive thresholding scheme. Gabor, Morlet, and anisotropic Gaussian filters were applied using the frequencies and bandwidths listed, and their outputs were fused by weighted averaging based on local coefficient energy. The fused coefficients were then inverted through the curvelet synthesis step to obtain the final denoised image.

TABLE I. KEY PARAMETER SETTINGS USED IN MCF-DD

Component	Parameter	Value	Justification
Curvelet Transform [46]	Number of Scales (S)	4	Captures multi-scale features with balance between detail and computational cost.
Curvelet Transform [47]	Number of Orientations (N_θ)	8	Provides directional sensitivity while avoiding redundancy.
Gabor Filter [40]	Frequency	0.6	Optimized for texture preservation in noisy lung regions.
Morlet Filter [42]	Sigma	1.5	Balances frequency and spatial localization.
Anisotropic Gaussian [43]	σx, σy	(1.2, 2.0)	Emphasizes edge preserving smoothing.
Thresholding [47]	Adaptation Method	GMM based dynamic	Adapts to local statistics and noise intensity using data driven classification.

IV. RESULTS AND DISCUSSION

A. Patch-Based Classification Performance

To evaluate the performance of patch classification approach for the noise type classification, experiments were conducted on Chest X-Ray images from Kaggle dataset [8]. The evaluation is done for the categorization of Gaussian noise, Poisson noise and also for finding the noise free patches. The experiments were conducted by dividing the input image into 32 X 32 patches and 64 x 64 patches. A synthetic noise generation strategy was employed to create patch level ground truth labels, as no publicly available Chest X-Ray dataset includes annotations identifying the dominant noise type at the patch-level.

A set of high-quality Chest X-Ray images with minimal visible noise was selected as the baseline reference, serving as the clean images for controlled noise synthesis. Gaussian noise was added using predefined mean and variance parameters, while Poisson noise was introduced based on fixed photon intensity distributions. A subset of patches was intentionally left unaltered to represent clean regions. Because each noise type was assigned deterministically during the synthesis process, precise and unambiguous ground truth labels could be maintained for every patch. The results were plotted in Fig. 4 and Patch classification is calculated by using Eq. (13) [48]:

$$\text{Accuracy} = \frac{\text{Correctly Classified Patches}}{\text{Total Patches}} \times 100\% \quad (13)$$

From Fig. 4, we can infer that larger patches improves classification accuracy. This suggests that larger patches retain more structural and statistical information, making it easier to distinguish noise patterns. The improvement in accuracy with 64×64 patches highlight their effectiveness in preserving spatial features critical for classification.

B. MCF-DD Performance

The experimental results demonstrate the effectiveness of the proposed denoising technique, Multi-Scale Curvelet Filtering with Directional Denoising in comparison to selected denoising methods.

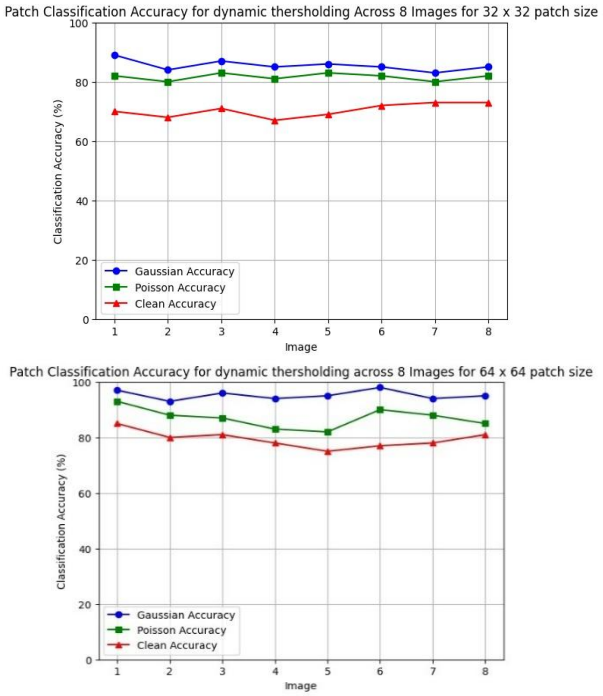

Fig. 4. Effect of patch size on classification accuracy.

Experimental study was performed on images from the Chest X-Ray Images dataset collected from the Kaggle repository [8], in which the chest radiographs are present in JPEG format. To analyze the impact of compression artifacts experimental study was also performed on the DICOM format CXR images from the Medical Imaging Data Resource Center (MIDRC) – RSNA International COVID Radiology Database (RICORD) Release 1c [9]. The MIDRC-RICORD-1C dataset provides high quality DICOM images, allowing for a more comprehensive evaluation of the denoising performance on uncompressed medical images.

To evaluate the robustness of the proposed denoising methodology, synthetic noise was added to the clean Chest X-Ray images. Specifically, Gaussian noise with a pre-defined mean of zero and variance σ2 = 0.01 was applied to simulate additive noise commonly encountered in imaging systems. Additionally, Poisson noise was introduced based on the intensity distribution of each image to replicate the photon counting noise inherent in X-ray acquisition processes. These noise models allow us to simulate realistic degradation scenarios for comprehensive evaluation. All denoisers were executed under identical noise conditions and preprocessing. Classical baselines followed standard reference implementations such as BM3D with σ matched to the corruption level, NLM with a 7×7 patch and 21×21 search window, and Wavelet denoising using soft threshold $\lambda = 3\sigma$. DnCNN was evaluated using its publicly released pretrained Gaussian model with inputs normalized to [0,1]. GAN-based baselines were retrained on the same noisy clean pairs used in the proposed work, by using U Net generator, Patch GAN discriminator, Adam optimizer (LR = 2×10^{-4}), and 100 training epochs with 256×256 patches. All methods were run on identical hardware and image sizes for consistent comparison. PSNR and SSIM are used in this study to assess denoising performance at the pixel and structural levels, and diagnostic evaluation of the proposed framework has been reported previously [49].

1) Peak Signal-to-Noise Ratio (PSNR): This metric is used to measure the quality of a denoised image compared to the original image, as shown in Eq. (14) [48]. The quality of the denoised image increases as the PSNR value increases.

$$PSNR = 10log_{10}(M^2/MSE) \quad (14)$$

2) Structural Similarity Index (SSIM): This metric is used to calculate the structural similarity between the denoised image and the original image. It is calculated by comparing different image features such as pixelpatterns, luminance, pixel intensities, etc as given in Eq. (15) [37].

$$\mathrm{SSIM}(x,y) = \frac{(2\mu_x\mu_y+C_1)(2\sigma_{xy}+C_2)}{(\mu_x^2+\mu_y^2+C_1)(\sigma_x^2+\sigma_y^2+C_2)} \quad (15)$$

where, x and y are the two images being compared. The constants C1 and C2 used in the SSIM calculation follow standard values as originally proposed in [37], typically set as $C1 = (K_1L)^2$ and $C2 = (K_2L)^2$, where $K_1 = 0.01$, $K_2 = 0.03$, and L is the dynamic range of pixel values.

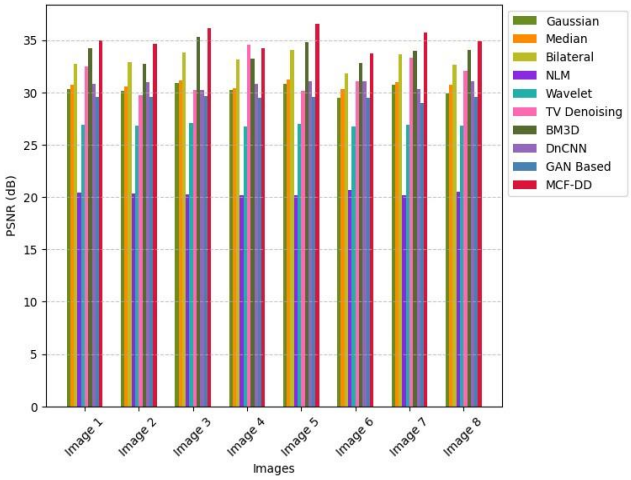

Fig. 5. PSNR comparison of denoising approaches with the proposed method, MCF-DD [Chest X-Ray Dataset].

In Fig. 5, the PSNR value obtained by the proposed MCF-DD method and the other state-of-the-art methods for denoising images from the chest X-ray data set are plotted. The results indicate that the proposed method yields a higher PSNR rate compared to the other existing methods. In Table II, the comparison of the proposed method to the other methods using the images from Chest X-Ray Dataset is given. The lower performance of NLM is mainly due to oversmoothing of fine anatomical details and reduced effectiveness in handling mixed noise, leading to lower PSNR values compared with the proposed transform-based framework. For deep learning-based denoising methods, the dataset was divided into training, validation, and testing subsets with proportions of 70%,15%, and 15%, respectively, using stratified random sampling to maintain class balance. To prevent data leakage, images from the same patient were included in only one of these subsets.

Synthetic noisy images were generated independently by adding the same noise models (Gaussian noise with zero mean and variance σ2 = 0.01, and Poisson noise based on image intensity) to the clean images in each subset. The deep learning models were trained exclusively on the noisy images from the training set, using the corresponding clean images as ground truth. Evaluation was performed on the noisy images in the testing set, ensuring no overlap or exposure of test data during training. This protocol guarantees a fair and unbiased comparison between deep learning and traditional denoising methods under consistent noise conditions.

Similarly, in Fig. 6, the SSIM values of the denoised image obtained by the proposed method and other techniques using images from the Chest X-Ray Dataset are represented. The higher the SSIM value index, the better the performance in preserving the structure of the denoised image. The proposed method has the highest SSIM values when compared with the SSIM values obtained by other methods.

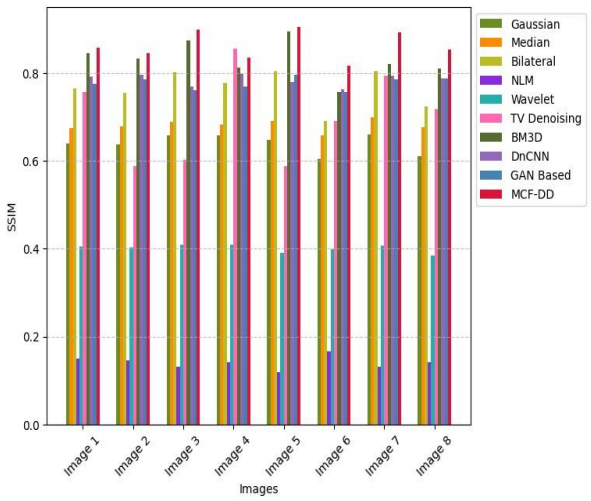

Fig. 6. SSIM comparison of denoising approaches with the proposed method, MCF-DD [Chest X-Ray dataset].

TABLE II. COMPARISON OF DENOISING APPROACHES WITH THE PROPOSED METHOD, MCF-DD [CHEST RAY DATASET].

Denoised Method	Evaluation	Image I	Image II	Image III	Image IV	Image V	Image VI	Image VI	Image V111
	PSNR	27.56	27.10	27.81	26.49	27.17	28.08	27.30	27.38
Noisy Image	SSIM	.4843	.4688	.4786	.4175	.4062	.5747	.4430	.4983
	PSNR	30.30	30.12	30.91	30.21	30.80	29.44	30.69	29.93
Gaussian [13]	SSIM	.6399	.6380	.6585	.6577	.6487	.6057	.6608	.6118
	PSNR	30.72	30.59	31.16	30.36	31.20	30.29	30.98	30.76
Median [14]	SSIM	.6747	.6781	.6893	.6833	.6915	.6589	.6986	.6779
	PSNR	32.70	32.92	33.82	33.11	34.05	31.81	33.67	32.61
Bilateral [15]	SSIM	.7648	.7554	.8030	.7772	.8043	.6914	.8049	.7245
	PSNR	20.39	20.36	20.27	20.15	20.15	20.65	20.17	20.54
NLM [16]	SSIM	.1506	.1454	.1304	.1417	.1178	.1657	.1311	.1421
	PSNR	26.87	26.83	27.05	26.75	26.96	26.71	26.91	26.84
Wavelet [20]	SSIM	.4060	.4023	.4090	.4087	.3909	.3993	.4063	.3853
	PSNR	32.46	29.76	30.23	34.54	30.15	31.04	33.29	32.08
TV Denoising [50]	SSIM	.7570	.5874	.6032	.8564	.5892	.6906	.7944	.7179
	PSNR	34.20	32.68	35.30	33.25	34.84	32.79	34.00	34.01
BM3D [51]	SSIM	.8456	.84343	.8742	.8123	.8943	.7582	.8202	.8099
	PSNR	30.80	31.00	30.25	30.82	31.02	31.08	30.31	31.06
DnCNN [30]	SSIM	.7930	.7958	.7705	.7990	.7800	.7633	.7944	.7874
	PSNR	29.57	29.59	29.61	29.46	29.56	29.46	329.02	29.54
GAN based [31]	SSIM	.7750	.7870	.7610	.7694	.7964	.7583	.7871	.7873
	PSNR	34.96	34.63	36.17	34.23	36.57	33.69	35.70	34.89
MCF-DD	SSIM	.8584	.8452	.8996	.8362	.9062	.8175	.8935	.8536

To understand the better performance of the proposed MCF-DD, the visual results obtained by processing a noisy image using both MCF-DD and other methods are shown in Fig. 7.

Even tough Chest X-Ray Datasets are widely used for medical image analysis, the resultant JPEG compression artifacts may cause unwanted noise that may not be present in the actual image. To perform a more realistic assessment of the performance of the proposed method, uncompressed DICOM images were included from the Medical Imaging Data Resource Center (MIDRC) – RSNA International COVID Radiology Database (RICORD) Release 1c (MIDRC-RICORD-1C) [9]. This dataset, curated by MIDRC and RSNA, consists of high-resolution clinically acquired CXR images stored in DICOM format, preserving the original image quality without lossy compression artifacts. The inclusion of DICOM images allows for a more reliable evaluation of real-world noise characteristics that are typically encountered in medical imaging. In Table III, the comparison of the proposed method with the other methods using images from the (MIDRC) - RSNA International COVID Radiology Database (RICORD) is given.

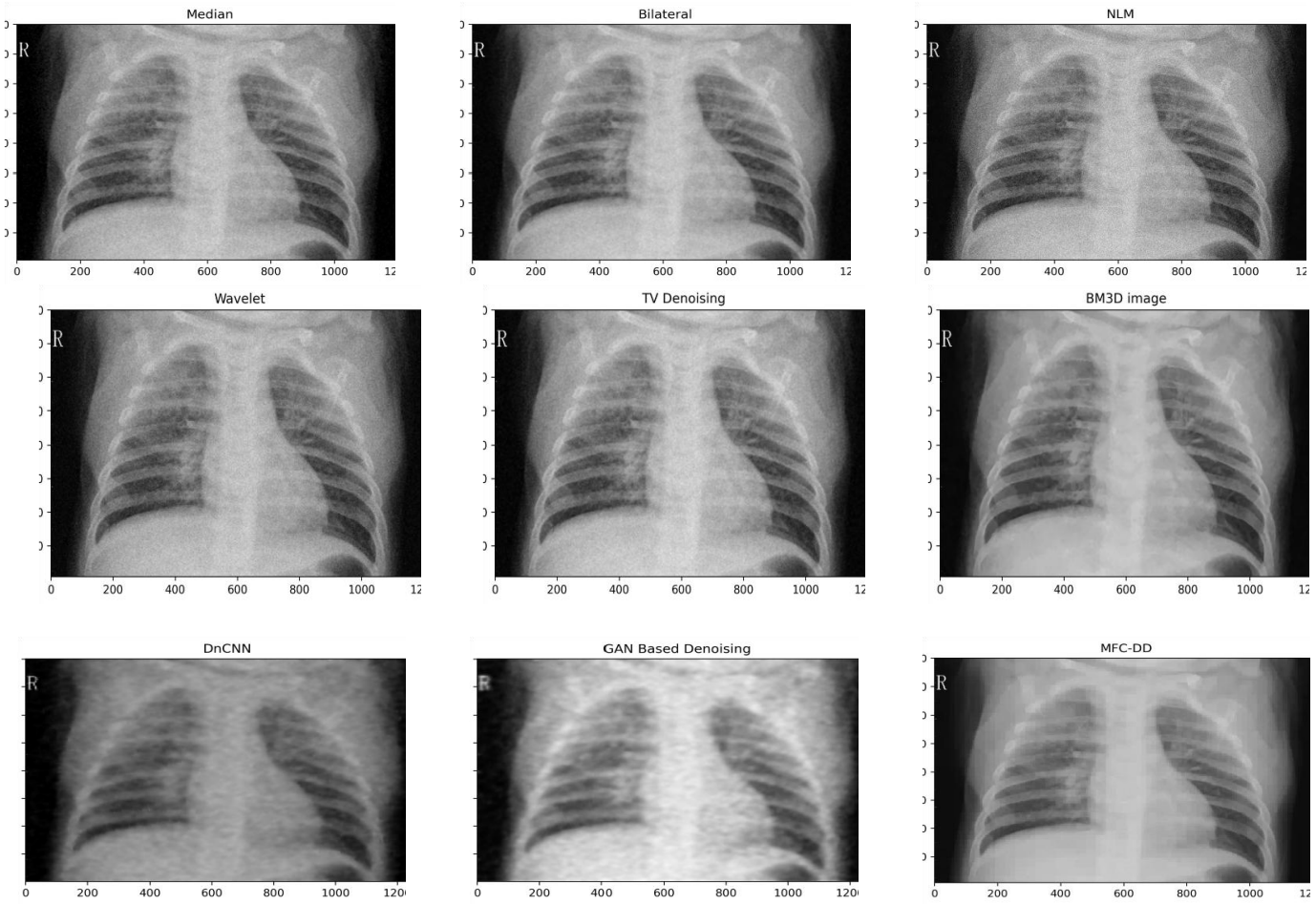

Fig. 7. Visual comparison of denoising methods applied to chest x-ray images [Chest X- Ray Dataset].

TABLE III. COMPARISON OF DENOISING APPROACHES WITH THE PROPOSED METHOD, MCF-DD [(MIDRC) -RSNA INTERNATIONAL 382 COVID RADIOLOGY DATABASE].

Denoised method	Evaluation criteria	Image I	Image II	Image III	Image IV	Image V	Image VI	Image VII	Image VIII
Noisy Image	PSNR	28.21	28.58	27.01	27.93	27.49	25.41	27.17	25.93
	SSIM	.5087	.4704	.5191	.6688	.4714	.2701	.4346	.2824
Gaussian [13]	PSNR	30.07	30.73	29.89	28.33	30.14	36.14	30.50	30.28
	SSIM	.5815	.6327	6390	.4954	.6055	.7685	.6173	.6154
Median [14]	PSNR	31.31	31.33	29.89	28.41	31.11	33.56	31.15	31.07
	SSIM	.6483	.6768	.6259	.4646	.6456	.8009	.6502	.6766
Bilateral [15]	PSNR	32.59	33.65	31.46	29.82	32.91	36.87	33.03	33.98
	SSIM	.7002	.7887	.6959	.5599	.7277	.8097	.7364	.7984
NLM [16]	PSNR	20.48	20.08	20.12	20.64	20.25	30.09	20.14	20.03
	SSIM	.1211	.1153	.1752	.2123	.1298	.2099	.1255	.1972
Wavelet [20]	PSNR	26.85	26.85	26.44	26.15	26.77	31.17	26.73	26.84
	SSIM	.3550	.3755	.4224	.3956	.3763	.6567	.3743	.3507
TV Denoising [50]	PSNR	33.80	33.35	32.31	29.40	29.70	33.45	32.68	29.98
	SSIM	.7790	.7744	.7365	.5375	.5569	.8709	.7313	.550
BM3D [51]	PSNR	33.03	35.90	30.50	29.73	33.06	31.73	34.67	34.38
	SSIM	.8398	.8561	.7161	.5945	.8007	.7589	.8872	.8672
DnCNN [30]	PSNR	30.20	29.67	28.40	29.22	27.71	29.51	30.10	28.11
	SSIM	.7493	.7675	.7343	.7862	.7235	.7634	.7474	.7913
GAN Based [31]	PSNR	27.68	27.40	26.79	27.15	26.86	25.84	27.19	27.02
	SSIM	.7387	.7621	.7340	.7733	.7184	.6984	.7577	.7575
MCF-DD	PSNR	36.34	37.24	32.51	31.01	35.17	38.92	35.51	40.04
	SSIM	.8621	.9089	.7365	.6756	.8267	.9119	.8361	.9476

Fig. 8 and Fig. 9 represent the comparison of the PSNR and SSIM values of the proposed method with the other existing methods for the experiments carried out on DICOM images. From the analysis, we can find that the performance of the

proposed method is better than that of the existing methods. MCF-DD method achieves the highest PSNR and SSIM values across different images. DICOM images are free of compression artifacts. The noise presenting DICOM images represents the original noise characteristics. Conventional denoising techniques have poor performance on DICOM images, while the proposed method adapts well to real X-ray noise patterns, rather than just compression noise.

The proposed MCF-DD (Multi Scale Curvelet based Filtering with Directional Denoising) method demonstrates improved performance for the denoising of chest X-Ray images by combining Curvelet Transform with multiple spatial frequency filters like Gabor, Morlet, and Anisotropic Gaussian, and using a Gaussian Mixture Model (GMM) for adaptive thresholding. The use of Curvelet Transform allows better handling of edges and directional features, which results in multi-scale feature preservation. Also, the combination of different filters helps to capture a wide range of textural and frequency information, contributing to effective noise suppression. The adaptive threshold selection avoids rigid assumptions about the noise model and adapts to local noise characteristics. Table IV presents a comparative analysis of the proposed multi-scale curvelet filtering with the directional denoising technique against existing methods. The results indicate that the proposed approach achieves the highest PSNR and SSIM, demonstrating superior denoising performance and preservation of structural fidelity compared to the state-of-the-art techniques.

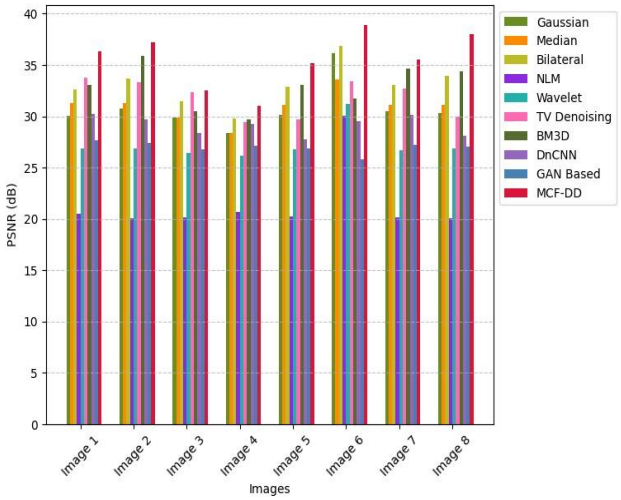

Fig. 8. PSNR comparison of denoising approaches with the proposed method, MCF-DD [(MIDRC) - RSNA International 382 COVID radiology database].

TABLE IV. COMPARISON OF DIFFERENT METHODS ON THE KAGGLE CHEST X-RAY DATASET

Study	Method used	PSNR	SSIM
CNN-based Pneumonia Detection [52]	Convolutional Neural Network (CNNs)	34.12	0.8734
Vision Transformers (ViT) [53]	Vision Transformer (ViT)	35.78	0.8941
Deep Learning Ensemble [54]	Ensemble of GoogLeNet, ResNet-18, DenseNet-121	34.89	0.8812
Hybrid Inception ResNet [55]	Fine-Tuned Inception-ResNet	35.95	0.8994
Proposed method	Multi-Scale Curvelet Filtering with Directional Denoising	**36.57**	**0.9062**

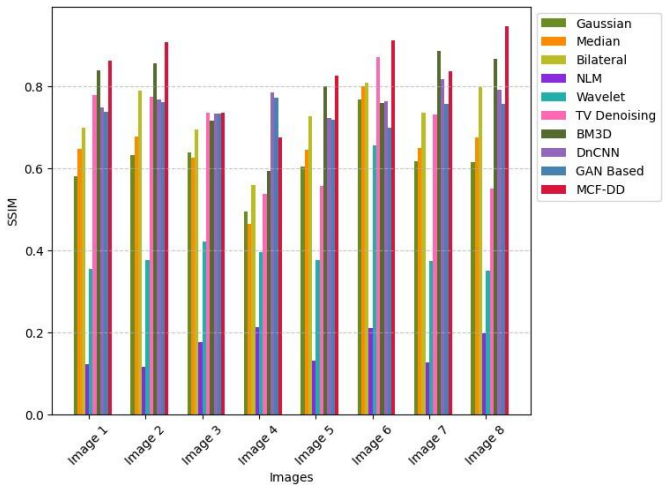

Fig. 9. SSIM comparison of denoising approaches with the proposed method, MCF-DD [(MIDRC) - RSNA International 382 COVID Radiology Database].

The drawbacks of the proposed method include sensitivity to parameter settings and increased computational complexity due to multiple filtering stages. Additionally, this method does not model inter scale dependencies, which may affect performance in highly textured regions. Another limitation of this study is the absence of a radiologist's evaluation to assess whether the denoised images lead to improved diagnostic interpretation. Future work will incorporate domain expert feedback using structured assessment methods, as employed in prior studies [56].

Although PSNR and SSIM are widely adopted for quantitative evaluation of image, they primarily reflect pixel level fidelity and structural similarity. Diagnostic evaluation of the proposed denoising framework has been reported in a previously published study [49], where MCF-DD processed chest X ray images were assessed using standard classification metrics. Accordingly, the present work employs PSNR and SSIM to analyze denoising effectiveness at the signal level.

C. Computational Efficiency Analysis

The runtime comparison presented in Table V indicates that simple local filtering methods such as Gaussian and median filtering have minimal computational cost but provide limited denoising capability. In contrast, non-local and optimization-based approaches, including BM3D and total variation denoising, exhibit substantially higher runtime due to exhaustive block matching and iterative optimization procedures. Learning-based methods reduce this overhead

through feed forward inference but, CNN and GAN-based denoisers still require higher processing time than the proposed framework. With an average inference time of 0.101 ± 0.013 s per image, the proposed MCF-DD method achieves a favorable balance between denoising effectiveness and computational efficiency, remaining significantly faster than BM3D and more efficient than CNN and GAN-based approaches, thereby demonstrating its suitability for large-scale chest X-ray preprocessing.

TABLE V. RUNTIME COMPARISON OF DENOISING METHODS

Method	Runtime (s/image)
Gaussian Filter	0.008 ± 0.009
Median Filter	0.008 ± 0.002
Bilateral Filter	0.075 ± 0.025
Wavelet Denoising	0.083 ± 0.018
Total Variation (TV)	0.760 ± 0.404
BM3D	5.76 ± 0.77
CNN	0.181 ± 0.087
GAN	0.198 ± 0.099
Proposed Method (MCF-DD)	**0.101 ± 0.013**

D. Contribution Analysis of MCF-DD Framework Components.

To understand the contribution of each processing component within the proposed MCF-DD framework, a comparative study was performed by progressively incorporating the framework components. The study began with the Curvelet Transform, which serves as the core multi-scale representation mechanism for noise suppression. Subsequently, the Gabor filter, Morlet filter, and anisotropic Gaussian filter were incrementally integrated into the framework. The average PSNR and SSIM values obtained from the evaluation images are summarized in Table VI.

TABLE VI. MCF-DD FRAMEWORK COMPONENT ANALYSIS

Configuration	PSNR (dB)	SSIM
Curvelet Transform	33.84 ± 0.42	0.861 ± 0.011
Curvelet Transform and Gabor Filter	34.71 ± 0.38	0.882 ± 0.010
Curvelet Transform and Gabor Filter and Morlet Filter	35.48 ± 0.34	0.894 ± 0.008
Curvelet Transform and Gabor Filter and Morlet Filter and Anisotropic Gaussian Filter (MCF-DD)	36.57 ± 0.21	0.906 ± 0.004

The Curvelet Transform alone achieved a PSNR of 33.84 dB and an SSIM of 0.861, demonstrating its effectiveness in suppressing noise while preserving major anatomical structures. When the Gabor filter was incorporated, the PSNR increased to 34.71 Db, and the SSIM improved to 0.882. This improvement can be attributed to the ability of the Gabor filter to capture directional texture information and enhance edge representation. The addition of the Morlet filter further improved performance, resulting in a PSNR of 35.48 dB and an SSIM of 0.894. The Morlet filter enhances multi-scale frequency representation and improves the preservation of subtle anatomical patterns commonly present in chest radiographs. Finally, the integration of the anisotropic Gaussian filter produced the complete MCF-DD framework. This stage effectively suppressed residual noise while preserving edge continuity and structural integrity. Consequently, the proposed MCF-DD framework achieved the highest performance, with a PSNR of 36.57 dB and an SSIM of 0.906.

V. CONCLUSION AND FUTURE SCOPE

In this study, a novel denoising method is introduced, Multi-Scale Curvelet Filtering with Directional Denoising (MCF-DD), along with a patch classification method. This method mainly focuses on the medical chest X-ray images, in which maintenance of structural information of both fine and larger image features is as important as denoising the Poisson and Gaussian noise. A key strength of the method is its dynamic noise classification strategy, powered by a Gaussian Mixture Model (GMM) applied on the variance-to-mean ratio of image patches, allowing adaptive and noise-specific processing. The experimental evaluation demonstrated that MCF-DD outperforms several traditional and state-of-the-art denoising techniques in terms of both quantitative metrics, such as PSNR and SSIM, and qualitative visual quality of the denoised images. The performance has been evaluated on compressed (JPEG) and uncompressed (DICOM) images from diverse datasets, including Kaggle CXR and MIDRC-RICORD.

The adaptability and robustness of the proposed MCF-DD method can be improved by integrating data-driven learning components, such as deep learning-based denoising priors. In addition, the parameter selection process can be automated using optimization algorithms or reinforcement learning frameworks to improve generalization. A critical extension is the integration of the MCF-DD pipeline within explainable AI frameworks to support clinical interpretability.

In summary, MCF-DD presents a flexible, adaptive, and effective solution for image denoising, particularly suited for challenging conditions such as mixed noise scenarios in medical imaging. The promising results lay the foundation for further research and real-world clinical applications.

ACKNOWLEDGMENT

The authors would like to thank the creators of the publicly available chest X-ray datasets used in this study for making the data accessible for research purposes

REFERENCES

[1] M. Diwakar et al., “Low-dose COVID-19 CT image denoising using CNN and its method noise thresholding,” Curr. Med. Imaging Rev., vol. 19, no. 2, pp. 182–193, 2023.

[2] H. Koyuncu and R. Ceylan, “Elimination of white Gaussian noise in arterial phase CT images to bring adrenal tumours into the forefront,” Comput. Med. Imaging Graph., vol. 65, pp. 46–57, 2018.

[3] S. Guo, G. Wang, L. Han, X. Song, and W. Yang, “COVID-19 CT image denoising algorithm based on adaptive threshold and optimized weighted median filter,” Biomed. Signal Process. Control, vol. 75, p. 103552, 2022.

[4] M. Klug et al., "Denoised Ultra-Low-Dose Chest CT to Assess Pneumonia in Individuals Who Are Immunocompromised," Radiol. Cardiothorac. Imaging, vol. 7, no. 2, p. e240189, 2025.

[5] S. V. M. Sagheer and S. N. George, "A review on medical image denoising algorithms," Biomed. Signal Process. Control, vol. 61, p. 102036, 2020.

[6] Rashid, N.; Berriri, K.; Albekairi, M.; Kaaniche, K.; Ben Atitallah, A.; Khan, M.A.; El-Hamrawy, O.I. New Real-Time Impulse Noise Removal Method Applied to Chest X-ray Images. Diagnostics 2022, 12, 2738. https://doi.org/10.3390/diagnostics12112738.

[7] J. Mohan, V. Krishnaveni, and Y. Guo, "A survey on the magnetic resonance image denoising methods," Biomed. Signal Process. Control, vol. 9, pp. 56–69, 2014.

[8] D. S. Kermany et al., "Identifying Medical Diagnoses and Treatable Diseases by Image-Based Deep Learning," Cell, vol. 172, no. 5, pp. 1122-1131.e9, Feb. 2018, doi: 10.1016/J.CELL.2018.02.010.

[9] E. Tsai et al., "Data from Medical Imaging Data Resource Center (MIDRC) – RSNA International COVID Radiology Database (RICORD) Release 1c – Chest x-ray, Covid+ (MIDRC-RICORD-1C)." The Cancer Imaging Archive, 2021, doi: 10.7937/91ah-v663.

[10] M. Diwakar and M. Kumar, "A review on CT image noise and its denoising," Biomed. Signal Process. Control, vol. 42, pp. 73–88, 2018.

[11] D. K. Priya, B. B. Sam, S. Lavanya, and A. P. Sajin, "A survey on medical image denoising using optimisation technique and classification," in 2017 international conference on information communication and embedded systems (ICICES), 2017, pp. 1–6, doi: 10.1109/ICICES.2017.8070729.

[12] L. Fan, F. Zhang, H. Fan, and C. Zhang, "Brief review of image denoising techniques," Vis. Comput. Ind. Biomed. Art, vol. 2, no. 1, p. 7, 2019.

[13] P. Chen, H. Qian, and M. Zhu, "Fast Gaussian particle filtering algorithm [J]," J. Huazhong Univ. Sci. \& Technol., 2008.

[14] T. Huang, G. Yang, and G. Tang, "A fast two-dimensional median filtering algorithm," IEEE Trans. Acoust., vol. 27, no. 1, pp. 13–18, 1979.

[15] D. Bhonsle, V. Chandra, and G. R. Sinha, "Medical image denoising using bilateral filter," Int. J. Image, Graph. Signal Process., vol. 4, no. 6, p. 36, 2012.

[16] A. Buades, B. Coll, and J.-M. Morel, "A non-local algorithm for image denoising," in 2005 IEEE computer society conference on computer vision and pattern recognition (CVPR'05), 2005, vol. 2, pp. 60–65, [Online]. Available: 10.1109/CVPR.2005.38.

[17] F. Jin, P. Fieguth, L. Winger, and E. Jernigan, "Adaptive Wiener filtering of noisy images and image sequences," in Proceedings 2003 International Conference on Image Processing (Cat. No. 03CH37429), 2003, vol. 3, pp. III--349.

[18] T. Barbu, "Robust anisotropic diffusion scheme for image noise removal," Procedia Comput. Sci., vol. 35, pp. 522–530, 2014.

[19] S. G. Chang, B. Yu, and M. Vetterli, "Adaptive wavelet thresholding for image denoising and compression," IEEE Trans. image Process., vol. 9, no. 9, pp. 1532–1546, 2000.

[20] D. L. Donoho, I. M. Johnstone, G. Kerkyacharian, and D. Picard, "Wavelet shrinkage: asymptopia?," J. R. Stat. Soc. Ser. B, vol. 57, no. 2, pp. 301–337, 1995.

[21] S. Hashemi and S. Beheshti, "Adaptive image denoising by rigorous Bayesshrink thresholding," in 2011 IEEE Statistical Signal Processing Workshop (SSP), Jun. 2011, pp. 713–716, doi: 10.1109/SSP.2011.5967802.

[22] M. S. Moad, N. Zermi, A. Khaldi, and M. R. Kafi, "Stationary wavelet-based image watermarking for E-healthcare applications," Cybern. Syst., vol. 56, no. 2, pp. 81–96, 2025.

[23] F. E. Ali, I. M. El-Dokany, A. A. Saad, and F. E. Abd El-Samie, "A curvelet transform approach for the fusion of MR and CT images," J. Mod. Opt., vol. 57, no. 4, pp. 273–286, 2010.

[24] J. K. Appati, B. Ziamah, H. A. Akrofi, and A. A. Dodoo, "SARS detection in chest CT scan images using the bootstrapped ViT-B/16 model," Iran J. Comput. Sci., pp. 1–15, 2025.

[25] Z. Zhang, J. Cui, X. Luo, and Q. You, "Statistical correlative model in the multimodal fusion of brain images," Int. J. Imaging Syst. Technol., vol. 30, no. 4, pp. 1066–1079, 2020.

[26] K. and K. F. and C. T. and K. A. and C. L. Zotin Alexanderand Simonov, "Techniques for Medical Images Processing Using Shearlet Transform and Color Coding," in Computer Vision in Control Systems-4: Real Life Applications, L. C. Favorskaya Margarita N.and Jain, Ed. Cham: Springer International Publishing, 2018, pp. 223–259.

[27] K. Zhang, W. Zuo, Y. Chen, D. Meng, and L. Zhang, "Beyond a gaussian denoiser: Residual learning of deep cnn for image denoising," IEEE Trans. image Process., vol. 26, no. 7, pp. 3142–3155, 2017.

[28] J. Lehtinen, "Noise2Noise: Learning Image Restoration without Clean Data," arXiv Prepr. arXiv1803.04189, 2018.

[29] M. Nishio et al., "Convolutional auto-encoder for image denoising of ultra-low-dose CT," Heliyon, vol. 3, no. 8, 2017.

[30] Murali Vineeth and P. V and Sudeep, "Image Denoising Using DnCNN: An Exploration Study," in Advances in Communication Systems and Networks, Jun. 2020, pp. 847–859, doi: https://doi.org/10.1007/978-981-15-3992-3_72.

[31] H.-J. Kim and D. Lee, "Image denoising with conditional generative adversarial networks (CGAN) in low dose chest images," Nucl. Instruments Methods Phys. Res. Sect. A Accel. Spectrometers, Detect. Assoc. Equip., vol. 954, p. 161914, 2020.

[32] M. Sandhu, S. Kushwaha, and T. Arora, "A Comprehensive Review of GAN-Based Denoising Models for Low-Dose Computed Tomography Images," Int. J. Image Graph., p. 2550030, 2023.

[33] K. Dabov, A. Foi, V. Katkovnik, and K. Egiazarian, "Image denoising by sparse 3D transform-domain collaborative filtering," IEEE Trans. Image Process., vol. 16, no. 8, pp. 2080–2095, 2007, doi: 10.1109/TIP.2007.901238.

[34] F. Deeba, S. Kun, F. A. Dharejo, and Y. Zhou, "Wavelet-based enhanced medical image super resolution," IEEE Access, vol. 8, pp. 37035–37044, 2020.

[35] N. Mohana Suganthi and M. Arun, "Diabetic retinopathy grading using curvelet CNN with optimized SSO activations and wavelet-based image enhancement," Ain Shams Eng. J., vol. 16, no. 1, p. 103239, 2025, doi: 10.1016/j.asej.2024.103239.

[36] M. Thelwall, "The precision of the arithmetic mean, geometric mean and percentiles for citation data: An experimental simulation modelling approach," J. Informetr., vol. 10, no. 1, pp. 110–123, Feb. 2016, doi: 10.1016/j.joi.2015.12.001.

[37] Z. Wang, A. C. Bovik, H. R. Sheikh, and E. P. Simoncelli, "Image quality assessment: From error visibility to structural similarity," IEEE Trans. image Process., vol. 13, no. 4, pp. 600–612, 2004.

[38] M. Qutbi, "On the Convergence of Maximum Likelihood Expectation--maximization Algorithm for Iterative Tomographic Reconstruction and the Role of Spatial Frequency, Location, Pixel Intensity, Contrast, and Noise," J. Med. Phys., vol. 50, no. 2, pp. 348–358, 2025.

[39] F. J. Anscombe, "The Transformation of Poisson, Binomial and Negative-Binomial Data," Biometrika, vol. 35, no. 3–4, pp. 246–254, Dec. 1948, doi: 10.1093/biomet/35.3-4.246.

[40] J. G. Daugman, "Two-dimensional spectral analysis of cortical receptive field profiles," Vision Res., vol. 20, no. 10, pp. 847–856, 1980.

[41] J. Zou, C.-C. Liu, Y. Zhang, and G.-F. Lu, "Object recognition using Gabor co-occurrence similarity," Pattern Recognit., vol. 46, no. 1, pp. 434–448, 2013.

[42] J. Morlet, G. Arens, E. Fourgeau, and D. Glard, "Wave propagation and sampling theory—Part I: Complex signal and scattering in multilayered media," Geophysics, vol. 47, no. 2, pp. 203–221, 1982.

[43] P. Perona and J. Malik, "Scale-space and edge detection using anisotropic diffusion," IEEE Trans. Pattern Anal. Mach. Intell., vol. 12, no. 7, pp. 629–639, 1990.

[44] D. L. Donoho and I. M. Johnstone, "Ideal spatial adaptation by wavelet shrinkage," Biometrika, vol. 81, no. 3, pp. 425–455, 1994.

[45] E. J. Candès and D. L. Donoho, "New tight frames of curvelets and optimal representations of objects with piecewise C2 singularities," Commun. Pure Appl. Math., vol. 57, no. 2, pp. 0219–0266, Feb. 2004, doi: 10.1002/cpa.10116.

[46] E. Candès, L. Demanet, D. Donoho, and L. Ying, "Fast Discrete Curvelet Transforms," Multiscale Model. \& Simul., vol. 5, no. 3, pp. 861–899, 2006, doi: 10.1137/05064182X.

[47] H. Wei and W. Zheng, "Image denoising based on improved gaussian mixture model," Sci. Program., vol. 2021, no. 1, p. 7982645, 2021.

[48] G. Litjens et al., "A survey on deep learning in medical image analysis," Med. Image Anal., vol. 42, pp. 60–88, Dec. 2017, doi: 10.1016/j.media.2017.07.005.

[49] N. Sebastian and B. Ankayarkanni, "Enhanced ResNet-50 with Multi-Feature Fusion for Robust Detection of Pneumonia in Chest X-Ray Images," Diagnostics, vol. 15, no. 16, p. 2041, 2025.

[50] B. Li and D. S. Que, "Medical Images Denoising Based on Total Variation Algorithm," Procedia Environ. Sci., vol. 8, pp. 227–234, Jan. 2011, doi: 10.1016/j.proenv.2011.10.037.

[51] I. Djurović, "BM3D filter in salt-and-pepper noise removal," EURASIP J. Image Video Process., vol. 2016, pp. 1–11, 2016.

[52] M. S. Al Reshan et al., "Detection of pneumonia from chest X-ray images utilizing mobilenet model," in Healthcare, 2023, vol. 11, no. 11, p. 1561.

[53] S. Singh, M. Kumar, A. Kumar, B. K. Verma, K. Abhishek, and S. Selvarajan, "Efficient pneumonia detection using Vision Transformers on chest X-rays," Sci. Rep., vol. 14, no. 1, p. 2487, 2024.

[54] R. Kundu, R. Das, Z. W. Geem, G.-T. Han, and R. Sarkar, "Pneumonia detection in chest X-ray images using an ensemble of deep learning models," PLoS One, vol. 16, no. 9, p. e0256630, 2021.

[55] M. Neshat, M. Ahmed, H. Askari, M. Thilakaratne, and S. Mirjalili, "Hybrid inception architecture with residual connection: fine-tuned Inception-ResNet deep learning model for lung inflammation diagnosis from chest radiographs," Procedia Comput. Sci., vol. 235, pp. 1841–1850, 2024.

[56] [G. Mehdipoor, F. Salmani, and A. Arjmand Shabestari, "Survey of practitioners' competency for diagnosis of acute diseases manifest on chest X-ray," BMC Med. Imaging, vol. 17, pp. 1–6, 2017.